Measurement of the Photoelectron Detection Efficiency of the HPD Anode

Public Note

Issue: 3
Revision: 2

Reference: LHCb-2009-038
Created: August 14, 2007
Last modified: November 18, 2009

Prepared by: Laurence Carson[a] [b], Andrew Pickford[a], Paul Soler[a]
[a]University of Glasgow, Glasgow, UK

LHCb-2009-038
23/11/2009

[b]Corresponding author

Abstract

This paper reports on measurements carried out on the Hybrid Photon Detectors (HPDs) of the LHCb RICH detectors. The purpose of these tests is to determine the photoelectron detection efficiency η of the HPD anode. Knowledge of η is required for an accurate simulation of the RICH detectors. It is found that this efficiency is $(93.3 \pm 0.7)\%$ for a 50 ns digital readout window, and $(87.9 \pm 1.4)\%$ for a 25 ns digital readout window. The 25 ns result exceeds the LHCb-RICH requirement of 85%, and is in agreement both with direct η measurements using preseries HPDs, and with indirect measurements from testbeams using preseries and production HPDs.

Document Status Sheet

1. Document Title: Measurement of the Photoelectron Detection Efficiency of the HPD Anode			
2. Document Reference Number: LHCb-2009-038			
3. Issue	**4. Revision**	**5. Date**	**6. Reason for change**
Draft	0	May 27, 2008	First version. Proper error calculations still needed.
Draft	1	August 17, 2009	Full draft, with corrections from Chris and Paul.
Draft	2	November 13, 2009	Final draft, with corrections from Thierry and Ken.

Contents

List of Figures

List of Tables

1 Introduction

The two RICH detectors [1, 2] of LHCb require 484 Hybrid Photon Detectors (HPDs) to detect the Cherenkov photons that are emitted by charged particles as they traverse the RICH. To allow for failure of HPDs during LHC data taking, a total of 550 HPDs were manufactured for LHCb (see [3] and references therein). All HPDs have now been manufactured and have undergone thorough quality assurance testing at the Photon Detector Test Facilities (PDTFs) at the University of Glasgow and the University of Edinburgh.

This paper describes measurements carried out on two HPDs at the PDTF at the University of Glasgow. The purpose of these measurements is to find the single photoelectron detection efficiency, η, of the HPD anode. This anode consists of a pixel detector array bump-bonded to a binary readout chip packaged into a ceramic carrier (see [4] and references therein). Knowledge of η is required for an accurate simulation of the RICH detectors. A direct measurement of η involves comparing the average number of photoelectrons seen by the readout chip to the number arriving at the backplane of the silicon sensor. Since the measurement at the backplane is the interesting and challenging part of the efficiency measurement, the whole measurement is known as the "backpulse" measurement.

Section 2 explains the importance of measuring the single photoelectron detection efficiency, and Section 3 describes the general principles of the method to directly measure it at the PDTF. Section 4 outlines the effects within the sensor that cause η to be less than unity. The experimental setup and data taking methodology used at the Glasgow PDTF to carry out the measurement of η are respectively outlined in Secs. 5 and 6. Section 7 contains the results from the η measurement, including a discussion of how the errors were calculated. Conclusions are given in Sec. 8.

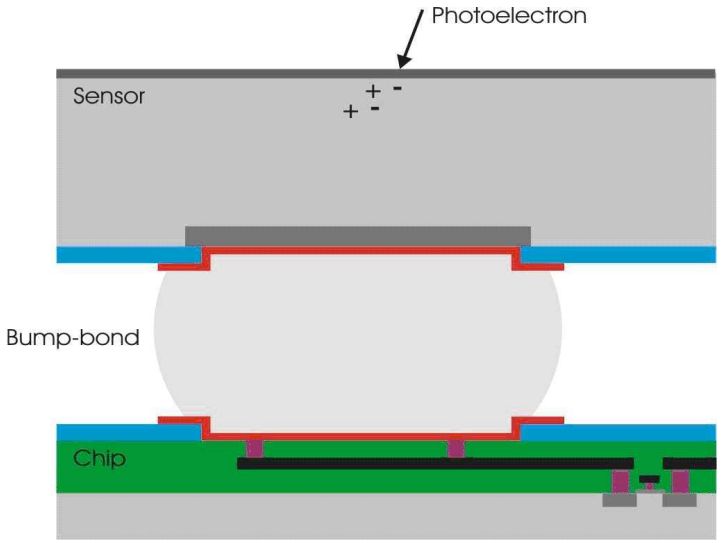

Figure 1 Diagram showing a Si pixel bump-bonded to a channel of the readout chip. At the top of the diagram is the sensor backplane, where the "analogue $\langle npe \rangle$" is measured. At the bottom of the diagram is the readout chip input stage, where the "digital $\langle npe \rangle$" is measured.

2 Why Measure the Photoelectron Detection Efficiency?

Given a saturated (i.e. $\beta \approx 1$) charged particle traversing a RICH detector, the expected number of hits N_{pe} expected in the photodetector plane is given by [5]

$$N_{pe} = \left(\frac{\alpha}{\hbar c}\right) L \epsilon_A \, \eta \int \mathcal{Q}\mathcal{R}\mathcal{T} \sin^2 \theta_c \, \mathrm{d}E_\gamma. \tag{1}$$

Apart from the leading factor, which is made up of fundamental physical constants, all the terms in Eqn. 1 are properties of the RICH system in question. The factors in front of the energy integral are the length L of the radiator, the fractional coverage ϵ_A provided by the photodetectors, and the single photoelectron detection efficiency η. The current note describes a direct measurement of η at the PDTF. It is also possible to make an indirect measurement of η in a testbeam setup, by measuring the average N_{pe} seen by the HPDs, and then using estimates for the other quantities in Eqn. 1 to deduce the value of η. The remaining terms are inside the integral as they are dependent on the energy of the emitted Cherenkov photon. They are the quantum efficiency $\mathcal{Q}$ of the HPD entrance window, the reflectivity $\mathcal{R}$ of the mirror system, the transmission $\mathcal{T}$ of the quartz window that encloses the photodetector system, and the Cherenkov angle θ_c. The salient feature of Eqn. 1 for the current study is that N_{pe} is directly proportional to η, which demonstrates that accurate knowledge of η is required to correctly reproduce N_{pe} in simulations of the RICH detectors. An accurate simulation of the detector is needed in order to correctly predict the detector performance, for example the PID likelihood distributions. So measuring η will improve the detector simulation, allowing the actual detector performance to be confidently compared to the predictions from the simulation, so that any discrepancies can be investigated.

3 How to Measure the Photoelectron Detection Efficiency

The method used here to measure η follows that described in detail in [6]. Light is shone onto the quartz window using a pulsed LED, producing photoelectrons inside the HPD vacuum. The number of photoelectrons produced is counted at two different areas of the HPD anode. These areas can be seen in Fig. 1. Firstly one counts the number of hits registered by the digital readout chip, as measured by the standard PDTF Labview software. This number is the "digital $\langle npe \rangle$", where $\langle npe \rangle$ means number of photoelectrons.

Secondly one counts the number of photoelectrons arriving at the backplane of the silicon sensor. This is done by measuring the current pulse induced on the backplane electrode, and inferring the amount of charge deposited there. Over a large number of events a histogram of the charge can be built up that should show peaks at multiples of the charge generated by one 20 keV photoelectron, which produces around 5,000 electron-hole pairs. The capacitive noise level associated with this measurement is very high, as the whole detector is being read out at once. This leads to a very large capacitance (proportional to the area being read out) of around 90 pF, compared to the 90 fF that is associated with an individual pixel. Using an appropriate fit to the charge distribution (see Sec. 6.2), one can deduce the average number of photoelectrons arriving at the backplane per LED strobe. This number is the "analogue $\langle npe \rangle$". The ratio of digital to analogue $\langle npe \rangle$ is the efficiency of the chip:

$$\eta = \frac{\langle npe \rangle_{\text{digital}}}{\langle npe \rangle_{\text{analogue}}}. \tag{2}$$

4 Factors Affecting Detection Efficiency

There are two main mechanisms by which the chip can fail to detect an incoming photoelectron, giving rise to an efficiency that is less than 100%. The first is called charge sharing. This occurs when a photoelectron hits the sensor near to the edge of a pixel, causing the electron-hole pairs to be detected by more than one pixel on the readout chip. It is possible for the electron-hole pairs to be shared between pixels in such a way that no individual pixel sees enough of a signal in the required time window to reach its discrimination threshold, so no pixel fires and the photoelectron is not detected by the chip.

The second, and predominant, mechanism is known as backscattering. When a photoelectron strikes a pixel on the sensor there is a chance that it will not deposit all of its energy there, but rather rebound from the sensor surface having deposited only part of its energy. This initial energy deposit may not be sufficient to reach the threshold and cause the pixel to fire. In this case several different scenarios are possible. If the backscattered photoelectron lands again outside of the detector chip, it will not be detected. If it lands again inside the detector chip, it may still be undetected, if its residual kinetic energy is below the discrimination threshold. The more likely outcome, given the typical threshold used in the HPD pixel chip, is that sufficient charge will be deposited at this stage to reach the threshold. However it is possible that by the time the photoelectron lands again and the charge from this second strike is collected, the readout window of the chip will have closed. In this case the photoelectron will be detected, but will be assigned to the wrong time window. This is known as a "timewalked" hit. Clearly the amount of timewalked hits depends strongly on the length of the readout window.

The probability that an electron striking a thick sensor will backscatter is a function only of the electron energy, angle of electron incidence and the atomic number of the sensor material [7]. Here, "thick" means sufficiently thick that the electron will not pass through the sensor. As the stopping range of a 20 keV electron in silicon is about 5 μm, this condition is comfortably satisfied for the case of the HPD sensor. For HPD operation, the electron energy (20keV) and atomic number of the sensor (14 for Si) are known, and the angle of incidence is restricted as the electron must originate at the HPD quartz window and strike the sensor. This means that the backscatter probability can be accurately estimated as 18%, with an error of less than 1% [7].

Note that both mechanisms described above depend on the length and position of the electronic "window" that defines when the chip is read out. This dependency will be explored in Section 7.3.

In addition to the above effects occuring within the HPD sensor, the observed photoelectron detection efficiency may also be affected by aspects of the measurement setup, such as the time distribution of the LED pulse. If this is too wide or contains a tail, this will increase the amount of hits seen in the wrong time window.

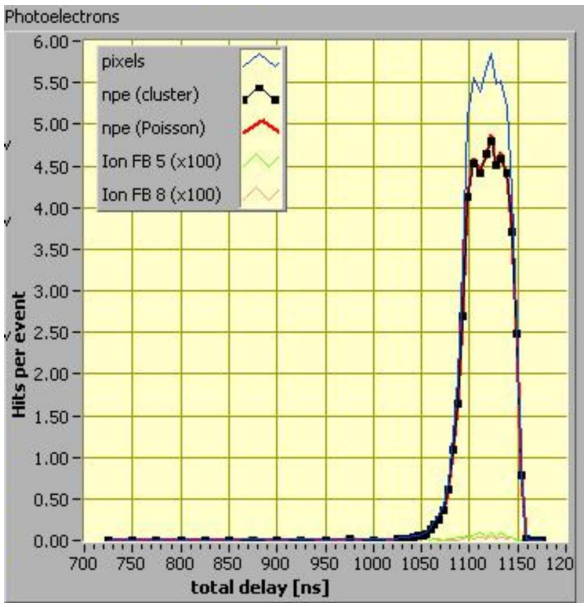

Figure 2 Screenshot of a typical strobescan. The delay shown refers to the trigger of the LED, so that a larger value corresponds to a shorter time between the LED firing and the chip being read out.

5 Backpulse Setup at PDTF

5.1 Digital Measurement

The digital $\langle npe \rangle$ is measured by running one of the standard software-based tests used in the PDTF characterisation program [8]. The test software is written in Labview [9] version 7.1. The particular test used is known as a strobescan. In the PDTF software, a clustering algorithm is used to form clusters from adjacent hit pixels. This gives a better estimate of the number of photoelectrons than simply counting pixels, as a single photoelectron can cause more than one pixel to fire via charge sharing (see Sec. 4). A strobescan measures the average number of clusters seen on the chip per LED trigger, as a function of the delay between the triggering of the LED and the readout of the chip. The relevant point on the strobescan for the η measurement is the point that gives the maximum number of clusters. This is the peak timing of the readout, which is what should be compared with the analogue $\langle npe \rangle$. Note that each point on the strobescan is measured by running 20,000 triggers. A screenshot of a typical strobescan is shown in Fig. 2.

The number of photoelectrons seen by the digital chip will depend on the length and position of the digital readout window. The digital readout window's position with respect to the signal from the chip can be modified via the standard PDTF Labview software. However the length of the window is hardwired into one of the chips on the PDTF electronics boards as 50 ns, and cannot be easily changed. The bunch crossing frequency of the LHC demands that a 25 ns-long window be used during LHCb data taking. Given the constraints on the window length that have just been mentioned, a 25 ns window is constructed by shifting the start of the 50 ns window back by 25 ns with respect to the signal, which leaves only the second 25 ns of the window with signal in it. It is expected that the η value obtained using the 50 ns gate will be larger than with the 25 ns gate, as the longer readout gate will pick up more timewalked hits (see Sec. 4).

5.2 Analogue Measurement

A schematic of the setup of the equipment used for the analogue measurement is shown in Fig. 3. The readout chain is operated as follows: the current pulse from the backplane is input to a low-noise charge preamplifier (model PR304 from Eurorad) that outputs a signal whose height is proportional to the amount of charge deposited at the backplane. To smooth this signal out it is passed through a commercial buffer amplifier (model EL2002CN from Elantec), then a fast filter amplifier (model 579

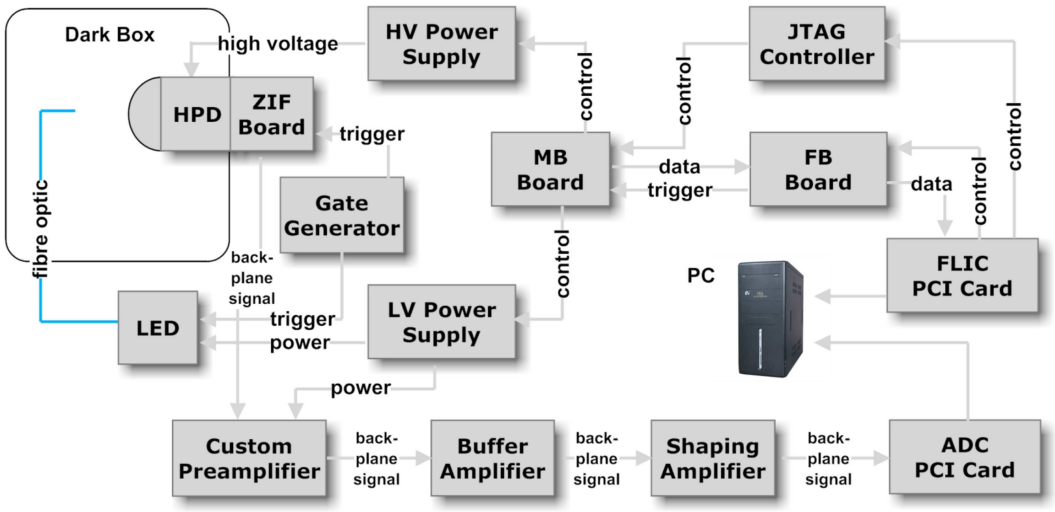

Figure 3 Schematic diagram of the setup for the measurement of the charge spectrum at the sensor backplane.

from Ortec). The shaping time of the Ortec amplifier is adjustable, and can take values between 10 ns and 500 ns. A shaping time of 200 ns was found to be optimal for data taking. Finally, the output of the Ortec amplifier is passed to a multi-channel analyser (Trump ADC card [10]) that is installed in a standard PC and is controlled using a software package called Maestro. The Maestro software produces a spectrum of counts versus channel number, where the channels correspond to different ADC values read out from the Trump card.

As mentioned above, the noise level in the analogue measurement is extremely high. If it is not minimised then the peak corresponding to each number of photoelectrons would be washed out of the spectrum so that they are not visible, and it would not be possible to make a reliable fit to the data. To minimise the noise level it was necessary to do the analogue measurement with the cables that are normally used to readout the chip disconnected. This removes the clocking noise from the readout boards that would otherwise swamp the backpulse signal. This strategy slows down the data taking process, as it means the system has to be powered down and up again between each analogue and digital measurement, but it is unavoidable. To minimise noise from electronic pickup, the dark box that houses the HPD during testing was covered with a wire mesh, which was grounded to the HPD high voltage ground. This effectively makes the dark box a Faraday cage. Use of the mesh was found to significantly reduce the noise seen on the backpulse signal.

The triggering of the LED and of the readout of the analogue signal are correlated using a chain of two gate generators. They are setup to allow the correct amount of time to elapse between firing the LED and reading out the resulting signal from the backplane. They also allow the starting point of the analogue readout gate and its length to be changed. This is important as the correct readout of the analogue signal is very sensitive to the exact setup of the analogue readout gate (see Section 6.6).

6 Procedure for Data Taking and Fitting

6.1 General Strategy

As the data taking procedure takes a finite amount of time, there will inevitably be changes in the environmental temperature. The size of the change in temperature depends on factors such as the time of day the measurement is carried out. Environmental temperature changes cause a change in the temperature of the LED, which in turn affects the average number of photons emitted by the LED each time it is triggered. To cope with this, one needs to monitor the changes in the LED output level over the time that the measurements are carried out. This is achieved by introducing a measurement procedure where each analogue measurement is sandwiched between two digital measurements. The

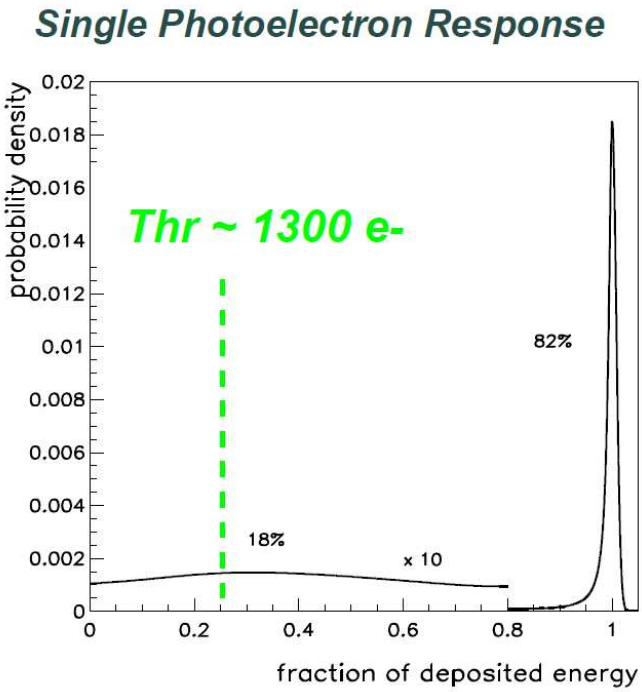

Figure 4 The single photoelectron response (SPR) of the HPD pixel chip. There is an 82% probability for the photoelectron to not backscatter, and so deposit all (or almost all) of its energy into the sensor upon striking it for the first time. If the photoelectron does backscatter (18% probability), the fraction of its energy that is deposited in the initial strike follows an approximately flat distribution (shown multiplied by a factor of 10 to make it visible). The green vertical line indicates the typical amount of charge required to be deposited in one pixel to cause it to fire. Reproduced from [11, 12].

average of the two digital $\langle npe \rangle$ is then taken as an estimate for what the digital $\langle npe \rangle$ would have been during the analogue measurement. From here on, $\bar{\mu}_{\rm dig}$ will be used to refer to the average digital $\langle npe \rangle$ (the value used to calculate η), while $\mu^1_{\rm dig}$ and $\mu^2_{\rm dig}$ will be used to refer to the digital $\langle npe \rangle$ measured by the first and second strobescans, respectively.

Demonstrating that the η value obtained for a given HPD is independent of the LED intensity (i.e. independent of the digital $\langle npe \rangle$) is vital in proving that a genuine efficiency is being measured. To check this, for each HPD studied measurements are performed at different levels of LED intensity. One can then check if the value of η changes with the LED intensity or not. However the LED intensity used should not be too high, to ensure that the probability of two or more photoelectrons striking the same pixel (thus distorting the measured digital $\langle npe \rangle$) remains very low.

6.2 Model for Charge Deposition Spectrum at Backplane

Before the analogue $\langle npe \rangle$ can be measured, a model needs to be defined that describes the sensor response to the arrival of a number of 20 keV photoelectrons at the backplane. This model will be used to perform a fit to the observed charge deposition spectrum, and extract the analogue $\langle npe \rangle$. The starting point for this model is the Single Photoelectron Response (SPR) function (see [12] and references therein). This describes the probability that a single photoelectron striking the sensor will deposit a certain fraction of its energy. The SPR for the HPDs was characterised previously by studying prototype HPDs that had a smaller pixel chip, and hence lower noise levels. In particular the spectra from these prototype HPDs have low enough noise levels such that a fit can be performed to measure the backscatter probability. The value found for the backscatter probability was around 18%, which is in agreement with the accepted value described in the previous section. The SPR used for the HPD pixel chip is shown in Figure 4.

The energy deposition spectrum for the arrival of two photoelectrons within the same readout window is just the convolution of the SPR with itself. This is because the arrival of photoelectrons is

independent. Another consequence of the independence of the photoelectrons is that the probability that a given number will arrive in the same time window follows a Poisson distribution. This is a key factor that allows the backpulse measurement to be carried out, as the relative height of each photoelectron peak will follow a Poisson distribution, whose mean μ is the analogue $\langle npe \rangle$.

So in the absence of noise in the readout chain, the charge spectrum would consist of a Poisson-weighted sum of the deposition spectrum for k electrons, where $k = \{1, 2, \ldots, \infty\}$ and the pedestal, which at this stage is just represented by a delta function at zero. Let this idealised charge spectrum be $f(x)$, where x represents the total charge deposited, in units of the charge generated by a single non-backscattered electron (which is ≈5,000 electrons). To account for the fact that there is electronic noise present both at the sensor and in the readout chain, one convolutes $f(x)$ with some global noise function $g(x)$ to obtain $h(x)$, say. This $h(x)$ is then a realistic model for the charge spectrum. In practice, $g(x)$ takes the form of a Gaussian. Applying a Fourier Transform to $h(x)$ gives (using the convention of capitalising transformed functions):

$$H(k) = F(k) \cdot G(k). \tag{3}$$

Under the assumption that the charge spectrum follows a Poisson distribution, it has been shown that a Light Sum Rule exists for the Fourier Transform of the charge spectrum [12]. The Light Sum Rule in this case gives

$$F(k) = \exp(\mu S(k)), \tag{4}$$

where μ is the Poisson mean, and $S(k)$ is the Fourier Transform of the SPR. The exponential arises as a power series formed by the addition in Fourier space of terms corresponding to each possible number of photoelectrons. The consequence of the Light Sum Rule is that one obtains a relatively simple expression for $H(k)$, and then one just applies the inverse Fourier Transform to obtain another relatively simple expression for $h(x)$, which now has an explicit dependence on μ, the variable of interest here. Hence performing the fit in Fourier space is faster and more robust than a brute force method of building the energy deposition spectrum from the SPR and the noise function without making use of the Light Sum Rule.

6.3 Pedestal Subtraction

During data taking it was observed that the height of the pedestal in each spectrum was always too large, i.e. the pedestal did not fit the Poisson distribution followed by the photoelectron peaks. The reason for this is not known, although it could be that, due to its peak-sensing nature, the ADC is picking up some dark count events. To deal with the excessive pedestal size, it was decided to remove the pedestal from each spectrum and fit to the modified spectrum using a model that also has the pedestal removed. This way the pattern of the photoelectron peaks is preserved, and these can be used to deduce the Poisson mean of the distribution. The pedestal subtraction process is illustrated in Figure 5.

To subtract the pedestal from a data spectrum, first a pedestal spectrum is taken to accompany each analogue run. This is done simply by taking an analogue run with the LED disabled. Then the pedestal spectrum is scaled so that it contains approximately the same number of events that comprise the pedestal contribution to the spectrum taken for the full analogue run. To carry out this scaling, the peak channel of the pedestal spectrum is first found, and the total number of counts in this channel and the eight surrounding channels (four channels each side) is calculated. The choice of taking four channels either side of the peak strikes a balance between the statistical fluctuations from using too few channels and dependence on the shape of the pedestal from using too many channels. The total number of counts in the corresponding channels of the full analogue spectrum is then calculated, and the scaling factor is found by taking the ratio of the these two numbers. This method relies on the fact that the mapping from channels to the peaks in the spectrum does not (for a given HPD) change from run to run.

Finally, the scaled pedestal is subtracted from the full analogue spectrum to give a spectrum consisting of only the photoelectron peaks. A modified fitting model is needed to cope with the pedestal-subtracted data. To subtract the pedestal from the fitting model, $F(k) - 1$ is substituted for $F(k)$ when constructing the fitting model (see Section 6.2).

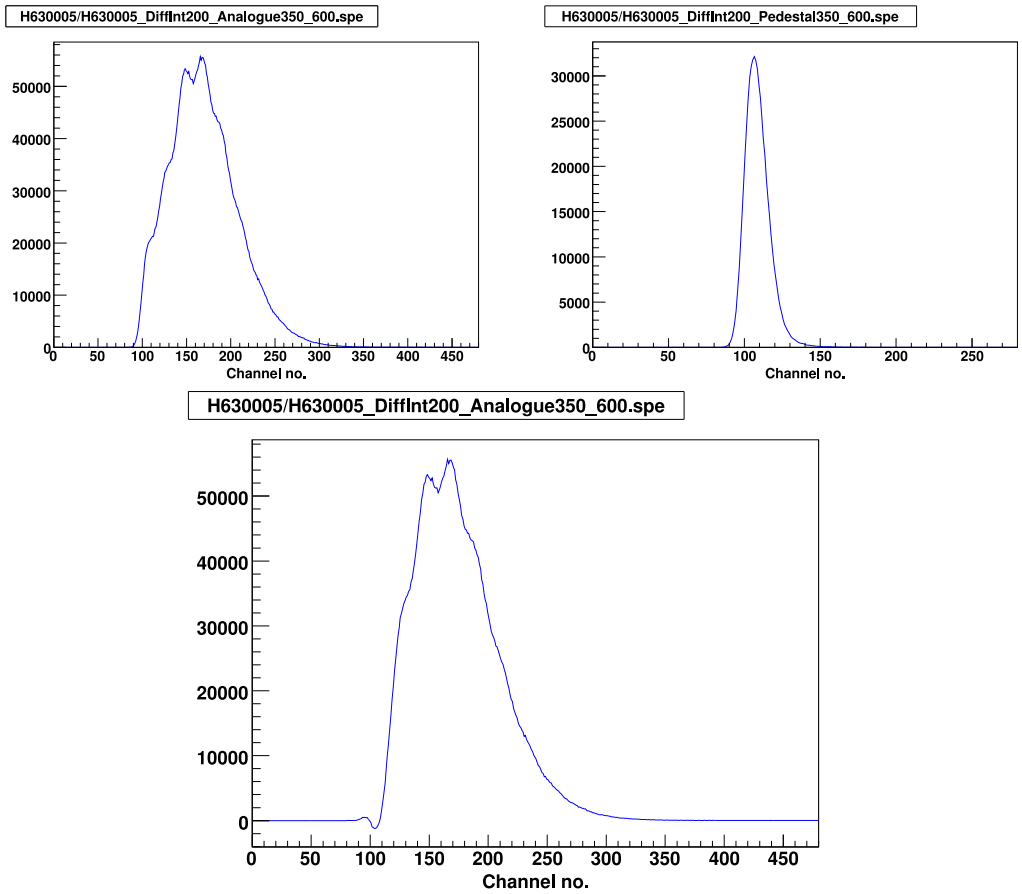

Figure 5 Analogue data taken from the sensor backplane. The blue line in each figure is formed from the histogram of the number of counts in each channel by linear interpolation. Top left: a "raw" spectrum including the pedestal. Top right: the corresponding pedestal-only run. It can be seen that the shape of the pedestal is asymmetric, which is a further indication that dark count events are being picked up. Bottom: the spectrum formed by scaling the pedestal and then subtracting it from the raw spectrum.

6.4 Fit Region

The fit region is defined as the channels for which the χ^2 between the data and the fit PDF is calculated during the fit. Fits including the pedestal region were often found to not converge correctly. This is because the distribution in the pedestal region is very sensitive to the pedestal scaling factor, the calculation of which is not an exact process. In particular negative values can be obtained after subtraction. Also, the fit region does not include the higher channels in the spectrum as the number of signal counts there is very low. Hence background noise in the readout chain can significantly distort the shape of the spectrum there, affecting in turn the fit to the lower photoelectron peaks. By contrast a small number of background counts at the lower photoelectron peaks will not affect the fit significantly, since most of the photoelectron data can be found in this region. For these reasons, the fit to the pedestal-subtracted spectrum is performed starting at the first or second photoelectron peak, and finishing at around the sixth or seventh photoelectron peak[a].

6.5 Execution of Fit

A fit is then performed using the modified model, $h(x)$, for the charge spectrum (see Sec. 6.2). The code used to carry out the fit was written in C++ by A. Pickford [13]. This code uses the "Simplex"

[a] However the fitting function is still drawn covering the whole spectrum to demonstrate that it is still in broad agreement with the spectrum even in the areas where the fit is not being done.

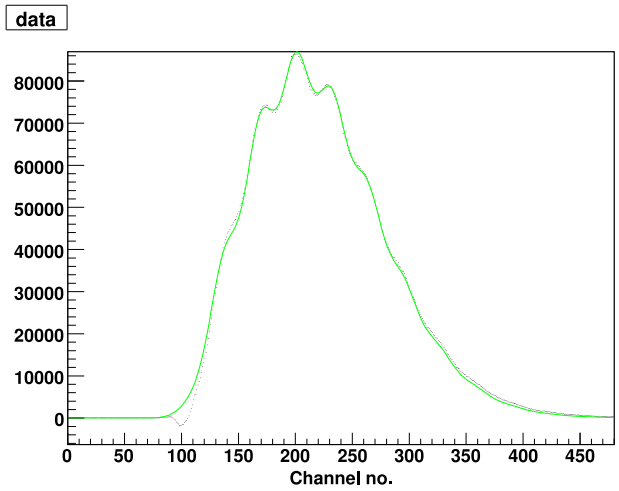

Figure 6 Typical fit to a backpulse spectrum with the pedestal subtracted. The data points are in black, and the fitted PDF is shown by the green line.

fitter from the GSL (GNU Scientific Library) package [14] to perform the minimisation. There are four parameters left floating in the fit: the location of the pedestal, the distance between photoelectron peaks, the width of the global noise Gaussian and the Poisson mean. As the location of the pedestal can be deduced within a few channels by inspecting the data, the fit is seeded with a value for the pedestal location that is very close to the full value. This prevents the fit from attempting to treat another photoelectron peak as the pedestal. The parameters of the SPR are fixed according to the results found from the fits to spectra from the prototype HPDs. An example fit is shown in Fig. 6.

6.6 Dependency of Efficiency on Analogue Gate

Data was taken with a number of different setups for the analogue gate. It was found that a strong dependence existed between the length of time the analogue gate extended after the peak of the signal. Note that this time is equivalent (modulo the signal rise time, which is independent of the gate setup) to the sum of the gate length and the delay between the start of the signal and the start of the gate. This dependency is shown in Figure 7.

It is found that having the gate extend roughly 500 ns after the signal peak gives values of the sensor efficiency (η) that are independent of the digital $\langle npe \rangle$ (see Figure 9), so this was chosen as the optimal gate setup. If the gate extends much more than 500 ns after the signal peak, then η is no longer independent of the digital $\langle npe \rangle$ (see Figure 7), while shorter gates do not give the ADC enough time to sample the signal fully[b], resulting in domination of the spectrum by the pedestal. The reason for the drop in analogue $\langle npe \rangle$ as the gate length increases is not fully understood. One possible cause is that the analogue signal is suffering some ringing after the main signal peak, but that this ringing is not large enough to show itself above the noise on the oscilloscope. The longer gate lengths include this ringing region of the signal, but the shorter ones do not. Another possible cause is an additional contribution from dark counts.

7 Results

Using the optimised analogue gate setup as described in Section 6.6, measurements were carried out on HPD H630005 using 25 ns and 50 ns digital gate lengths, and on HPD 708016 using 50 ns digital gate length. These particular HPDs were selected for this measurement as they exhibited excellent performance in the general PDTF tests. In particular, they have

[b]The documentation of the ADC states that the sampling gate must extend at least 500 ns after the peak of the signal for successful sampling of the whole of the signal to occur.

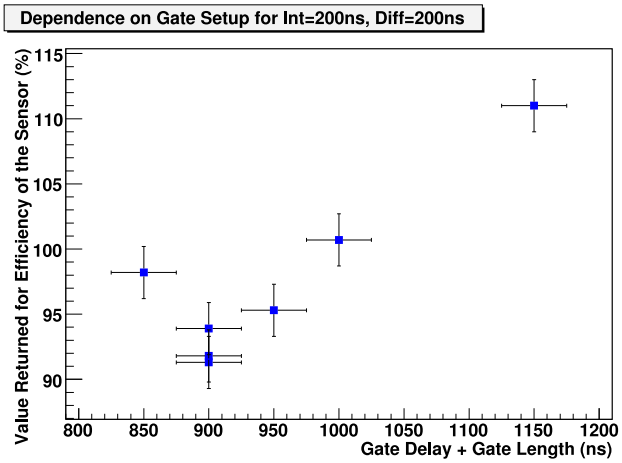

Figure 7 Dependence of the sensor efficiency (η) on analogue gate setup. Between "delay + length"= 900 ns and 1200 ns, there is a clear rise in the measured value of η. Below 900 ns, the gate does not last for long enough after the peak of the signal for the ADC to sample the full signal, and the size of the pedestal increases sharply, interfering with the rest of the photoelectron peaks.

- Very low leakage current ($\mathcal{O}$(10 nA)) from the detector chip, which minimises the shot noise,
- Very low dark-count rate ($\mathcal{O}$(1 kHz/cm^2)), which reduces the number of background hits on the detector chip,
- No dead or noisy pixels, to eliminate the need to take these into account when calculating the number of photoelectrons.

Since the pixel chip properties should vary little between HPDs, it is expected that no significant difference in η values will be seen between the two HPDs, and also that the η values obtained will be representative of the entire sample of HPDs.

7.1 Errors on Digital $\langle npe \rangle$

The statistical error on each of $\mu^1_{\rm dig}$ and $\mu^2_{\rm dig}$ (the digital measurements before and after the analogue measurement) is simply the uncertainty on the Poisson mean returned by the PDTF software. This can be estimated by calculating the increase in the χ^2 of the Poisson fit when a different Poisson mean is assumed, and choosing the variation in the mean that causes the χ^2 to increase by 1. This variation is found to range from 0.011 for low values of $\mu^{1,2}_{\rm dig}$ ($\simeq$2) to 0.017 for high values ($\simeq$6). The statistical error on $\bar{\mu}_{\rm dig}$ (the average digital $\langle npe \rangle$) is found by combining the errors on $\mu^{1,2}_{\rm dig}$ in quadrature, then halving the result. The typical statistical error is then around 0.01 or less. As will be seen below, this is small compared to the systematic error, and will be neglected.

The main systematic error on $\bar{\mu}_{\rm dig}$ comes from possible temperature-dependent changes in the LED output rate over time. Even when the difference between $\mu^1_{\rm dig}$ and $\mu^2_{\rm dig}$ is small, the output rate may for example have risen between the first strobescan and the analogue run, then fallen again between the analogue run and the second strobescan. To take this uncertainty into account, a systematic error is assigned to $\bar{\mu}_{\rm dig}$ as follows: the difference between $\mu^1_{\rm dig}$ and $\mu^2_{\rm dig}$ is calculated and halved. If the result is larger than 1% of $\bar{\mu}_{\rm dig}$, it is taken as the systematic error. Otherwise the systematic error is set to 1%. The choice of 1% as the minimum systematic uncertainty on $\overline{\mu}_{\rm dig}$ is based on the typical variations in digital $\langle npe \rangle$ that are seen between consecutive digital runs during normal HPD testing. Such variations can only be due to changes in the LED output rate.

This assignment leads to a systematic error of 1% for cases where $\mu^1_{\rm dig}$ and $\mu^2_{\rm dig}$ have very similar values, and of up to $\simeq$2% for cases where there was significant change between $\mu^1_{\rm dig}$ and $\mu^2_{\rm dig}$. So the systematic error on $\bar{\mu}_{\rm dig}$ is always at least several times larger than the statistical error, which is therefore neglected.

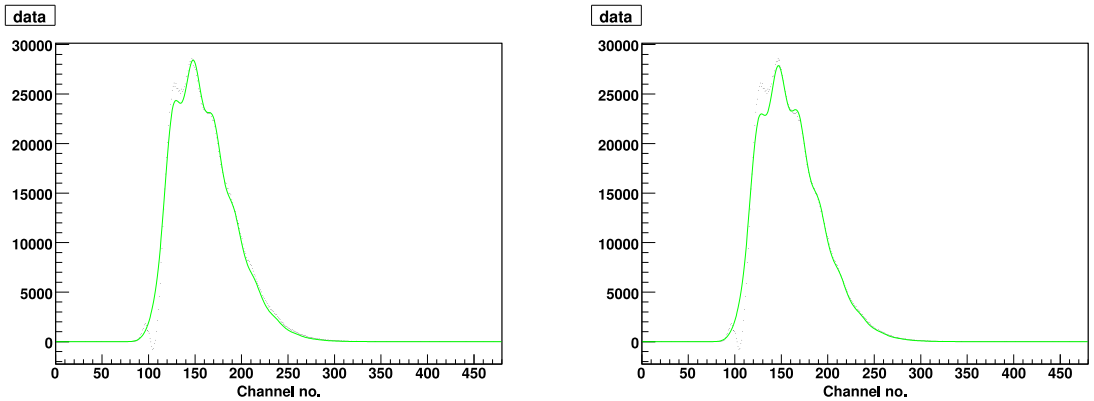

Figure 8 Effect of varying the fit region for a spectrum at low analogue $\langle npe \rangle$. The fit region for the left hand fit includes the first photoelectron peak, while the fit region for the right hand fit does not. The value of μ returned by the fit is 2.75 for the left hand fit and 2.86 for the right hand fit.

7.2 Errors on Analogue $\langle npe \rangle$

The statistical error on the analogue $\langle npe \rangle$ is the uncertainty on the μ parameter as returned by the fit to the backpulse spectrum. This can be estimated by the same method used for the digital $\langle npe \rangle$, by measuring how much each parameter must change to increase the total χ^2 of the fit by 1. For the μ parameter it is found that the change needed is of the order of 10^{-3}. This value is so small because the statistics present in a given spectrum are huge, with each bin of the early photoelectron peaks (see Fig. 6) holding of order 10^5 events. Thus the fractional error on the bin height is well below the percent level. The error returned by the fit is correspondingly very small. It will be seen below that this statistical error is completely negligible when compared to the systematic error. Hence the statistical error will not be considered when calculating the overall error on the analogue $\langle npe \rangle$.

A significant systematic error on the analogue $\langle npe \rangle$ arises because the model used to fit the backplane spectrum to extract μ does not accurately describe the data over the whole distribution. The size of the error introduced by this can be estimated in two different ways. Firstly, the change in μ caused by varying the region of the spectrum that is fitted to (i.e. the region where the χ^2 is calculated) can be studied. It is found that the largest change in μ is induced by not including the region of the first photoelectron peak in the fit. For most spectra this causes a change in μ of about 1%. But for spectra at low analogue $\langle npe \rangle$, the difference is more significant, at about 3%. A change of about 3% was also seen for the fits with the highest analogue $\langle npe \rangle$ values. The effect of changing the fit region on the fit result for a spectrum at low analogue $\langle npe \rangle$ is illustrated in Fig. 8. The fit on the left hand side is made including the first photoelectron peak in the fit region, while the fit region for the fit on the right hand side excludes the first photoelectron peak. It can be seen that the fit excluding the first photoelectron peak follows the data at the higher photoelectron peaks better, at the expense of a poorer fit at the first and second photoelectron peaks.

The second way of examining the effect of the imperfect fit on μ is to rerun the fit with one or more of the parameters that are normally floating being fixed, and examining how the fitted value for μ changes as the value chosen for the fixed parameter changes. The parameters representing the separation between photoelectron peaks and the location of the pedestal are varied within the ranges found when varying the fit region. This range is typically a few channels in size. These variations are found to cause a typical change in μ of around 1%. The size of this effect, unlike the effect of altering the fit region, does not significantly change from spectrum to spectrum.

The effect of choosing a different value for the backscattering probability in the SPR can also be considered. In light of the remarks about the backscattering probability in Sec. 4, 0.5% is chosen as an estimate of the uncertainty on the backscattering probability. Fitting with the probability fixed to be 0.5% either side of the 18% central value changes the fitted value of μ by about 0.4%. The size of this effect is independent of the spectrum studied. An error of this size can be neglected when compared with the other systematic uncertainties described above.

	Relative Error on Digital $\langle npe \rangle$	Relative Error on Analogue $\langle npe \rangle$	Relative Error on η
Statistical	$< 0.4\%$	$\mathcal{O}(0.1\%)$	$< 0.4\%$
Systematic	Between 1% and 2%, depending on $\lvert\mu^1_{\rm dig} - \mu^2_{\rm dig}\rvert$	Between 1.4% and 3.2%, depending on fit behaviour at first photoelectron peak	Between 1.7% and 3.7%
Combined	Between 1% and 2%	Between 1.4% and 3.2%	Between 1.7% and 3.7%

Table 1 Contributions to the total error on the sensor efficiency.

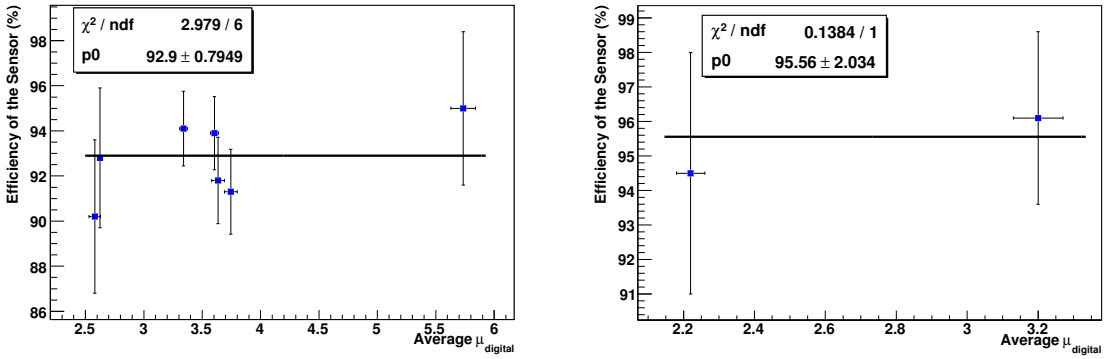

Figure 9 Results for η using digital gate length of 50 ns. The left hand plot shows results from HPD H630005, and the right hand plot shows results from HPD H708106.

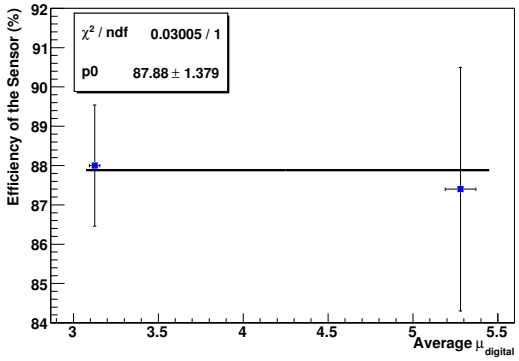

Figure 10 Results for η using digital gate length of 25 ns. Results are from HPD H630005.

As the statistical error on μ has also been seen to be negligible, the total error on μ is found by adding the two dominant systematic uncertainties, from variation of the fit region and of the other parameters in the fit, in quadrature.

7.3 Measured Values of the Detection Efficiency

The errors on digital $\langle npe \rangle$ and analogue $\langle npe \rangle$ are independent of each other. Hence the error on a single η value can be found by making use of Eqn. 2 to combine the digital and analogue errors:

$$\left(\frac{\sigma_\eta}{\eta}\right)^2 = \left(\frac{\sigma_{\langle npe \rangle_{\rm digital}}}{\langle npe \rangle_{\rm digital}}\right)^2 + \left(\frac{\sigma_{\langle npe \rangle_{\rm analogue}}}{\langle npe \rangle_{\rm analogue}}\right)^2 . \quad (5)$$

The contributions to the total error on η are summarised in Table 1. The results for η with 50 ns and 25 ns digital gate length are shown in Figs. 9 and 10 respectively.. In each plot in Figs. 9 and 10,

Digital Readout Window	Measured Value of η	LHCb-RICH Specification
50 ns	$(93.3 \pm 0.7)\%$	n/a
25 ns	$(87.9 \pm 1.4)\%$	85% typical

Table 2 Single photoelectron detection efficiency η of the manufactured HPDs, as measured at PDTF.

a constant fit has been made to give an average value for η from each plot. Performing a straight line fit shows that the gradient of η with respect to $\bar{\mu}_{\rm dig}$ is compatible with zero for all three plots, demonstrating that η is independent of $\bar{\mu}_{\rm dig}$ as desired.

Combining the results using digital gate length of 50 ns from the two HPDs allows overall results for both gate lengths to be stated. The errors are taken from the constant fits to each set of results. In Table 2 the overall results are given. The LHCb-RICH specification, which is governed by photoelectron backscattering effects and the expected performance of the pixel readout chip, is also given. As expected, the detection efficiency when using a 25 ns gate is significantly lower than when using a 50 ns gate. It can also be seen that the production HPDs exceed the LHCb-RICH requirement that the single photoelectron detection efficiency with a 25 ns readout window should have a typical value of 85%. The results are in agreement with η values that were measured using preseries HPDs [15], and with indirect measurements from testbeams using preseries [16] and production [17] HPDs.

8 Conclusions

The single photoelectron detection efficiency η of the LHCb HPD anode has been measured using two different digital readout windows. The efficiencies are found to be independent of the light input level, and in agreement with expectations from tests on preseries HPDs. The measured values are $\eta_{\rm 50ns} = (93.3 \pm 0.7)\%$ and $\eta_{\rm 25ns} = (87.9 \pm 1.4)\%$ respectively. This confirms that the production HPDs exceed the LHCb-RICH requirement in this respect. The value for the 25 ns gate will be used to optimise the simulation of the RICH detectors.

9 References

[1] LHCb Collaboration, *LHCb RICH Technical Design Report*, CERN LHCC 2000-037 LHCb, September 2000.

[2] LHCb Collaboration, *The LHCb Detector at the LHC*, 2008 JINST 3 S08005 (2008); `http://www.iop.org/EJ/journal/-page=extra.lhc/jinst`.

[3] T. Gys, *Production of 500 pixel hybrid photon detectors for the RICH counters of LHCb*, Nucl. Instr. Meth. **A 567** (2006) 176.

[4] K. Wyllie, *The front-end electronics of the LHCb ring-imaging-Cherenkov system*, Nucl. Instr. Meth. **A 567** (2006) 184.

[5] T. Ypsilantis and J. Seguinot, Nucl. Instr. Meth. **A 343** (1994) 30.

[6] M. Alemi *et al*, *First operation of a hybrid photon detector prototype with electrostatic cross-focussing and integrated silicon pixel readout.*, Nucl. Instr. Meth. **A 449** (2000) 48.

[7] E.H. Darlington, *Backscattering of 10–100 keV electrons from thick targets*, J.Phys. D: Applied Phys. **Vol. 8** (1975) 85.

[8] J. McCarron, *Characterisation of Hybrid Photon Detectors for the LHCb and an analysis of the rare decay $B_s \to \phi\phi$*, PhD Thesis, University of Edinburgh, April 2008. CERN-THESIS-2008-031.

[9] National Instruments LabVIEW Page. `http://www.ni.com/labview/`

[10] ORTEC TRUMP PCI. `http://www.ortec-online.com/trump.htm`

[11] M. Moritz, *Die LHCb RICH Pixel HPDs*, Talk given at Deutsche Physikalische Gesellschaft Frühjahrstagung des Fachverbandes Teilchenphysik 2004, 29 March–1 April 2004, Mainz, Germany.

[12] T. Tabarelli de Fatis, *Light Spectra Sum Rule*, Nucl. Instr. Meth. **A 385** (1997) 366.

[13] A. Pickford, Private Communication.

[14] GSL — GNU Scientific Library. `http://www.gnu.org/software/gsl/`

[15] M. Moritz *et al*, *Performance Study of New Pixel Hybrid Photon Detector Prototypes for the LHCb RICH Counters*, IEEE Trans. Nucl. Sci. **Vol. 51** (2004) 3.

[16] M. Adinolfi *et al*, *Performance of the LHCb RICH photodetectors in a charged particle beam*, Nucl. Instr. Meth. **A 574** (2007) 39.

[17] M. Adinolfi *et al*, *Performance of the LHCb RICH photo-detectors and readout in a system test using charged particles from a 25 ns-structured beam*, Nucl. Instr. Meth. **A 603** (2009) 287.